Geomechanics and Engineering, *Vol. 12*, *No. 2* (*2017*) *327-346*
DOI: https://doi.org/10.12989/gae.2017.12.2.327

Buckling analysis of embedded laminated plates with agglomerated CNT-reinforced composite layers using FSDT and DQM

Maryam Shokravi *

Buein Zahra Technical University, *Buein Zahra*, *Qazvin*, *Iran*

(*Received October 13*, *2016*, *Revised December 30*, *2016*, *Accepted January 05*, *2017*)

Abstract. Laminated plates have many applications in different industrials. Buckling analysis of these structures with the nano-scale reinforcement has not investigated yet. However, buckling analysis of embedded laminated plates with nanocomposite layers is studied in this paper. Considering the single-walled carbon nanotubes (SWCNTs) as reinforcement of layers, SWCNTs agglomeration effects and nonlinear analysis using numerical method are the main contributions of this paper. Mori-Tanaka model is applied for obtaining the equivalent material properties of structure and considering agglomeration effects. The elastic medium is simulated by spring and shear constants. Based on first order shear deformation theory (FSDT), the governing equations are derived based on energy method and Hamilton's principle. Differential quadrature method (DQM) is used for calculating the buckling load of system. The effects of different parameters such as the volume percent of SWCNTs, SWCNTs agglomeration, number of layers, orientation angle of layers, elastic medium, boundary conditions and axial mode number of plate on the buckling of the structure are shown. Results indicate that increasing volume percent of SWCNTs increases the buckling load of the plate. Furthermore, considering agglomeration effects decreases the buckling load of system. In addition, it is found that the present results have good agreement with other works.

Keywords: buckling of laminated plates; SWCNT; agglomeration effects; DQM; elastic medium

1. Introduction

Composite materials are widely used in many branches of industry such as aerospace, civil, naval and other high-performance engineering applications due to the high stiffness-to-weight ratio. The mechanical behaviors of laminated composite plates are strongly dependent on the degree of orthotropy of individual layers, the low ratio of transverse shear modulus to the in-plane modulus and the stacking sequence of laminates. A clear understanding on the mechanical analysis of laminated structures is required to achieve the full range of capabilities on the exemplary performance of laminated composite/sandwich structures. Hence, the buckling of laminated plates with nanocomposite layers in order to achieve the high stiffness is presented in this article.

With respect to the mechanical analysis of plates, Heydari *et al*. (2014) studied an analytical approach for transverse bending analysis of an embedded symmetric laminated rectangular plate using Mindlin plate theory and the surrounding elastic medium simulated using Pasternak

*Corresponding author, Ph.D., E-mail: Maryamshokravi10@gmail.com; Maryamshokravi10@bzte.ac.ir

http://www.techno-press.org/?journal=gae&subpage=7 ISSN: 2005-307X (Print), 2092-6219 (Online)

foundation. A cell-based smoothed discrete shear gap method (CS-FEM-DSG3) based on the first-order shear deformation theory (FSDT) was proposed by Phung-Van *et al*. (2014a) for static and dynamic analyses of Mindlin plates. Free vibration analysis of cracked Mindlin plates by integrating the original smoothed discrete shear gap method (CS-DSG3) with discontinuous and crack-tip singular enriched functions of the extended finite element method (XFEM) to give a so-called extended cell-based smoothed discrete shear gap method (XCS-DSG3) was presented by Nguyen-Thoi *et al*. (2014a). The edge-based strain smoothing technique was combined by Nguyen-Thoi *et al*. (2014b) with the three-node Mindlin plate element (MIN3) to give a so-called the edge-based smoothed three-node Mindlin plate element (ES-MIN3) for static and free vibration analyses of plates. A novel and effective formulation that combines the eXtended IsoGeometric Approach (XIGA) and higher-order shear deformation theory (HSDT) was proposed by Tran *et al*. (2015a) to study the free vibration of cracked functionally graded material (FGM) plates. A simple hyperbolic shear deformation theory taking into account transverse shear deformation effects was proposed by Saidi *et al*. (2016) for the free flexural vibration analysis of thick functionally graded plates resting on elastic foundations. Equilibrium and stability equations of functionally graded material (FGM) plate under thermal environment were formulated by Tran *et al*. (2016) in this paper based on isogeometric analysis (IGA) in combination with HSDT. An exact analytical solution for thermal stability of solar functionally graded rectangular plates subjected to uniform, linear and non-linear temperature rises across the thickness direction was developed by El-Hassar *et al*. (2016). The nonlinear transient formulation for plates was formed by Phung-Van *et al*. (2016) in the total Lagrange approach based on the von Kármán strains, which includes thermo-piezoelectric effects, and solved by Newmark time integration scheme. Based on the modified couple stress theory with only one material length scale parameter, the size-dependent behaviours of functionally graded microplates was studied by Nguyen *et al*. (2017).

In the field of composite plates, the CS-FEM-DSG3 was incorporated by Nguyen-Thoi *et al*. (2013) with spring systems for dynamic analyses of composite plates on the Pasternak foundation subjected to a moving mass. The CS-FEM-DSG3 was extended by Phung-Van *et al*. (2014b) to the layerwise deformation theory for dynamic response of sandwich and laminated composite plates resting on viscoelastic foundation subjected to a moving mass. The smoothed finite element method using three-node Mindlin plate element (CS-FEM-MIN3) was extended and incorporated by Luong-Van *et al*. (2014) with damping-spring systems for dynamic responses of sandwich and laminated composite plates resting on viscoelastic foundation subjected to a moving mass. Static and free vibration analyses of composite and sandwich plates were investigated by Phung-Van *et al*. (2014c) using the smoothed stabilized discrete shear gap method (ES-DSG3). An effectively numerical approach based on IGA and HSDT was presented by Tran *et al*. (2015b) for geometrically nonlinear analysis of laminated composite plates. Static and dynamic behaviors of functionally graded carbon nano-reinforced composite plates were studied by Phung-Van *et al*. (2015a) based on IGA and HSDT. In another work by Phung-Van *et al*. (2015b), dynamic control of smart piezoelectric composite plates was analyzed based on a generalized unconstrained approach in conjunction with IGA. Considering continuity of the displacement and transverse shear stresses at the layer interfaces, Tran *et al*. (2016) presented a generalized layerwise higher-order shear deformation theory for laminated composite and sandwich plates. In another work by Tran *et al*. (2016), a new simple four-unknown shear and normal deformations theory (sSNDT) for static, dynamic and buckling analyses of FGM isotropic and sandwich plates was presented.

However, buckling analysis of nanocomposite laminated plates has not been studied by the researchers. In the present study, the orthotropic Mindlin plate theory is used for nonlinear

buckling behavior of embedded laminated plates with nanocomposite layers. The layers are reinforced with the agglomerated SWCNTs where the Mori-Tanaka model is applied for nanocomposite layers. After deriving the governing equations by energy method and Hamilton's principal, DQM is applied for obtaining the buckling load of structure. The effects of the volume percent of SWCNTs, SWCNTs agglomeration, number of layers, orientation angle of layers, boundary conditions, elastic medium and axial mode number of plate on the buckling of the structure are disused in detail.

2. Mori-Tanaka Model and agglomeration effects

In this section, the effective modulus of the laminated plate reinforced by SWCNTs is developed based on Mori-Tanaka method. The matrix is assumed to be isotropic and elastic, with the Young's modulus E_m and the Poisson's ratio υ_m. The experimental results show that the assumption of uniform dispersion for nanoparticles in the matrix is not correct and the most of nanoparticles are bent and centralized in one area of the matrix. These regions with concentrated nanoparticles are assumed to have spherical shapes, and are considered as "inclusions" with different elastic properties from the surrounding material. The total volume V_r of nanoparticles can be divided into the following two parts (Shi and Feng 2004).

$$V_r = V_r^{inclusion} + V_r^m \tag{1}$$

where $V_r^{inclusion}$ and V_r^m are the volumes of nanoparticles dispersed in the spherical inclusions and in the matrix, respectively. Introduce two parameters ξ and ζ describe the agglomeration of nanoparticles

$$\xi = \frac{V_{inclusion}}{V}, \tag{2}$$

$$\zeta = \frac{V_r^{inclusion}}{V_r}. \tag{3}$$

However, the average volume fraction C_r of nanoparticles in the composite is

$$C_r = \frac{V_r}{V}. \tag{4}$$

Assume that all the orientations of the nanoparticles are completely random. Finally, the elastic modulus (E) and poison's ratio (υ) can be calculated as

$$E = \frac{9KG}{3K + G}, \tag{5}$$

$$\upsilon = \frac{3K - 2G}{6K + 2G}. \tag{6}$$

where the effective bulk modulus (K) and effective shear modulus (G) are expressed in Appendix

A. However, using Eqs. (5) and (6), the elastic constants of the structure can be calculated which are introduced in the next section.

3. FSDT

Based on FSDT, the displacement field can be written as (Heydari *et al*. 2014)

$$\begin{aligned} u_x(x,y,z,t) &= u\ (x,y,t) + z\psi_x(x,y,t), \\ u_y(x,y,z,t) &= v(x,y,t) + z\psi_y(x,y,t), \\ u_z(x,y,z,t) &= w(x,y,t), \end{aligned} \tag{7}$$

where (u_x, u_y, u_z) denote the displacement components at an arbitrary point (x, y, z) in the plate, and (u, x, w) are the displacement of a material point at (x, y) on the mid-plane (i.e. z = 0) of the plate along the x-, y-, and z-directions, respectively; ψ_x (x, y) and ψ_y (x, y) are the rotations of the normal to the mid-plane about x- and y- directions, respectively. The von Kármán strains associated with the above displacement field can be expressed in the following form

$$\varepsilon_{xx} = \frac{\partial u}{\partial x} + \frac{1}{2}\left(\frac{\partial w}{\partial x}\right)^2 + z\frac{\partial \psi_x}{\partial x}, \tag{8a}$$

$$\varepsilon_{yy} = \frac{\partial v}{\partial y} + \frac{1}{2}\left(\frac{\partial w}{\partial y}\right)^2 + z\frac{\partial \psi_y}{\partial y}, \tag{8b}$$

$$\gamma_{yz} = \frac{\partial w}{\partial y} + \psi_y, \tag{8c}$$

$$\gamma_{xz} = \frac{\partial w}{\partial x} + \psi_x, \tag{8d}$$

$$\gamma_{xy} = \frac{\partial v}{\partial y} + \frac{\partial u}{\partial x} + \frac{\partial w}{\partial x}\frac{\partial w}{\partial y} + z\left(\frac{\partial \psi_x}{\partial y} + \frac{\partial \psi_y}{\partial x}\right), \tag{8e}$$

where (ε_{xx}, ε_{yy}) are the normal strain components and (γ_{yz}, γ_{xz}, γ_{xy}) are the shear strain components. However, the constitutive equation for stresses σ and strains ε matrix of the kth layer can be expressed as follows (Reddy 1984)

$$\begin{Bmatrix} \sigma_{xx} \\ \sigma_{yy} \\ \sigma_{xy} \\ \sigma_{xz} \\ \sigma_{yz} \end{Bmatrix}^{(k)} = \begin{bmatrix} Q_{11} & Q_{12} & Q_{16} & 0 & 0 \\ Q_{12} & Q_{22} & Q_{26} & 0 & 0 \\ Q_{16} & Q_{26} & Q_{66} & 0 & 0 \\ 0 & 0 & 0 & Q_{55} & Q_{45} \\ 0 & 0 & 0 & Q_{45} & Q_{44} \end{bmatrix}^{(k)} \begin{Bmatrix} \varepsilon_{xx} \\ \varepsilon_{yy} \\ \gamma_{xy} \\ \gamma_{xz} \\ \gamma_{yz} \end{Bmatrix}^{(k)}, \tag{9}$$

where Q_{ij} (i, j = 1, 2,..., 6) are defined in Appendix B.

4. Governing equations

An embedded laminated plate with the nanocomposite layers which are reinforced with agglomerated SWCNTs is shown in Fig. 1. The geometrical parameters of laminated plate are length a, width b and total thickness h. The elastic medium is simulated by transverse shear loads (k_g) and normal loads (k_w).

The strain energy, U of the structure can be written as

$$U = \frac{1}{2}\int_V \left(\sigma_{xx}^{(k)}\varepsilon_{xx} + \sigma_{yy}^{(k)}\varepsilon_{yy} + \sigma_{xy}^{(k)}\gamma_{xy} + \sigma_{xz}^{(k)}\gamma_{xz} + \sigma_{yz}^{(k)}\gamma_{yz}\right)dV . \tag{10}$$

Combining of Eqs. (8)-(10) yields

$$\begin{aligned} U = \frac{1}{2}\int_{\Omega_0}\Bigg(& N_{xx}\left(\frac{\partial u}{\partial x} + \frac{1}{2}\left(\frac{\partial w}{\partial x}\right)^2\right) + N_{yy}\left(\frac{\partial v}{\partial y} + \frac{1}{2}\left(\frac{\partial w}{\partial y}\right)^2\right) + Q_y\left(\frac{\partial w_0}{\partial y} + \psi_y\right) + Q_x\left(\frac{\partial w_0}{\partial x} + \psi_x\right) \\ & + N_{xy}\left(\frac{\partial v}{\partial y} + \frac{\partial u}{\partial x} + \frac{\partial w}{\partial x}\frac{\partial w}{\partial y}\right) + M_{xx}\frac{\partial \psi_x}{\partial x} + M_{yy}\frac{\partial \psi_y}{\partial x} + M_{xy}\left(\frac{\partial \psi_x}{\partial y} + \frac{\partial \psi_y}{\partial x}\right)\Bigg)dxdy, \end{aligned} \tag{11}$$

where the stress resultant-displacement relations can be defined as

$$\left\{(N_{xx}, N_{yy}, N_{xy}), (M_{xx}, M_{yy}, M_{xy})\right\} = \sum_{k=1}^{N}\int_{z_{(k-1)}}^{z_{(k)}}\left\{\sigma_{xx}, \sigma_{yy}, \tau_{xy}\right\}(1, z)dz , \tag{12}$$

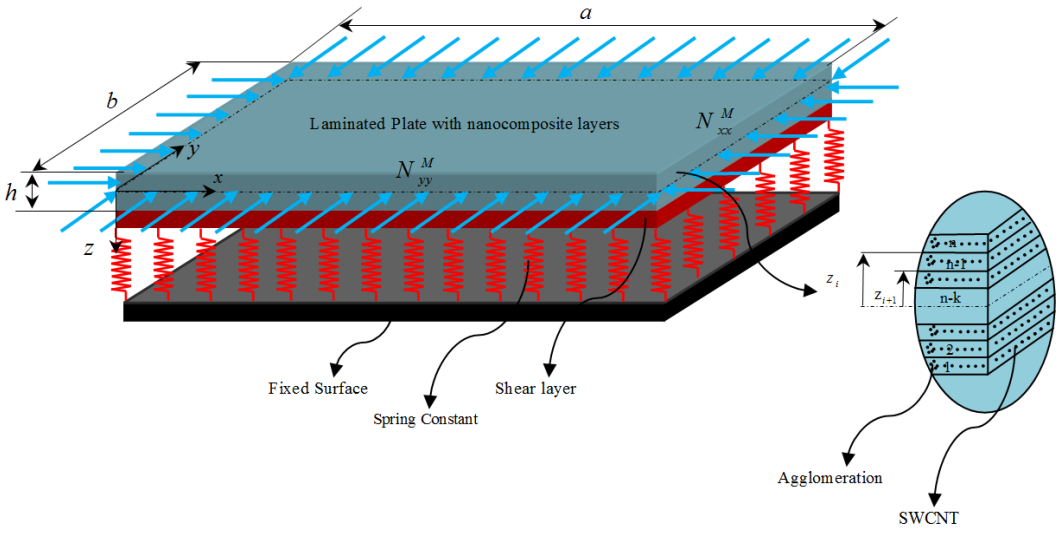

Fig. 1 The embedded laminated plate with agglomerated SWCNTs-reinforced layers

$$\left\{Q_x, Q_y\right\} = K\sum_{k=1}^{N}\int_{z^{(k-1)}}^{z^{(k)}}\left\{\sigma_{xz}, \sigma_{yz}\right\}dz, \tag{13}$$

in which K is shear correction coefficient.

The external work due to surrounding elastic medium can be written as (Heydari *et al*. 2014)

$$\delta u: \frac{\partial N_{xx}}{\partial x} + \frac{\partial N_{xy}}{\partial y} = 0, \tag{14}$$

$$\delta v: \frac{\partial N_{xy}}{\partial x} + \frac{\partial N_{yy}}{\partial y} = 0, \tag{15}$$

$$\delta w: \frac{\partial Q_x}{\partial x} + \frac{\partial Q_y}{\partial y} + \frac{\partial}{\partial x}\left(N_{xx}^{M}\frac{\partial w}{\partial x}\right) + \frac{\partial}{\partial y}\left(N_{yy}^{M}\frac{\partial w}{\partial y}\right) - k_w w + k_g\nabla^2 w = 0, \tag{16}$$

$$\delta\psi_x: \frac{\partial M_{xx}}{\partial x} + \frac{\partial M_{xy}}{\partial y} - Q_x = 0, \tag{17}$$

$$\delta\psi_y: \frac{\partial M_{xy}}{\partial x} + \frac{\partial M_{yy}}{\partial y} - Q_y = 0. \tag{18}$$

where N_{xx}^{M} and N_{yy}^{M} are the mechanical forces. Substituting Eqs. (8) and (9) into Eqs. (12) and (13), the stress resultant-displacement relations can be obtained as follow

$$\begin{aligned} N_{xx} &= A_{11}\left(\frac{\partial u}{\partial x} + \frac{1}{2}\left(\frac{\partial w}{\partial x}\right)^2\right) + A_{12}\left(\frac{\partial v}{\partial y} + \frac{1}{2}\left(\frac{\partial w}{\partial y}\right)^2\right) + A_{16}\left(\frac{\partial u}{\partial y} + \frac{\partial v}{\partial x} + \frac{\partial w}{\partial x}\frac{\partial w}{\partial y}\right) \\ &+ B_{11}\frac{\partial\psi_x}{\partial x} + B_{12}\frac{\partial\psi_y}{\partial y} + B_{16}\left(\frac{\partial\psi_x}{\partial y} + \frac{\partial\psi_y}{\partial x}\right), \end{aligned} \tag{19a}$$

$$\begin{aligned} N_{yy} &= A_{12}\left(\frac{\partial u}{\partial x} + \frac{1}{2}\left(\frac{\partial w}{\partial x}\right)^2\right) + A_{22}\left(\frac{\partial v}{\partial y} + \frac{1}{2}\left(\frac{\partial w}{\partial y}\right)^2\right) + A_{26}\left(\frac{\partial u}{\partial y} + \frac{\partial v}{\partial x} + \frac{\partial w}{\partial x}\frac{\partial w}{\partial y}\right) \\ &+ B_{12}\frac{\partial\psi_x}{\partial x} + B_{22}\frac{\partial\psi_y}{\partial y} + B_{26}\left(\frac{\partial\psi_x}{\partial y} + \frac{\partial\psi_y}{\partial x}\right), \end{aligned} \tag{19b}$$

$$\begin{aligned} N_{xy} &= A_{16}\left(\frac{\partial u}{\partial x} + \frac{1}{2}\left(\frac{\partial w}{\partial x}\right)^2\right) + A_{26}\left(\frac{\partial v}{\partial y} + \frac{1}{2}\left(\frac{\partial w}{\partial y}\right)^2\right) + A_{66}\left(\frac{\partial u}{\partial y} + \frac{\partial v}{\partial x} + \frac{\partial w}{\partial x}\frac{\partial w}{\partial y}\right) \\ &+ B_{16}\frac{\partial\psi_x}{\partial x} + B_{26}\frac{\partial\psi_y}{\partial y} + B_{66}\left(\frac{\partial\psi_x}{\partial y} + \frac{\partial\psi_y}{\partial x}\right), \end{aligned} \tag{19c}$$

$$M_{xx} = B_{11}\left(\frac{\partial u}{\partial x}+\frac{1}{2}\left(\frac{\partial w}{\partial x}\right)^2\right)+B_{12}\left(\frac{\partial v}{\partial y}+\frac{1}{2}\left(\frac{\partial w}{\partial y}\right)^2\right)+B_{16}\left(\frac{\partial u}{\partial y}+\frac{\partial v}{\partial x}+\frac{\partial w}{\partial x}\frac{\partial w}{\partial y}\right)$$
$$+D_{11}\frac{\partial \psi_x}{\partial x}+D_{12}\frac{\partial \psi_y}{\partial y}+D_{16}\left(\frac{\partial \psi_x}{\partial y}+\frac{\partial \psi_y}{\partial x}\right), \tag{20a}$$

$$M_{yy} = B_{12}\left(\frac{\partial u}{\partial x}+\frac{1}{2}\left(\frac{\partial w}{\partial x}\right)^2\right)+B_{22}\left(\frac{\partial v}{\partial y}+\frac{1}{2}\left(\frac{\partial w}{\partial y}\right)^2\right)+B_{26}\left(\frac{\partial u}{\partial y}+\frac{\partial v}{\partial x}+\frac{\partial w}{\partial x}\frac{\partial w}{\partial y}\right)$$
$$+D_{12}\frac{\partial \psi_x}{\partial x}+D_{22}\frac{\partial \psi_y}{\partial y}+D_{26}\left(\frac{\partial \psi_x}{\partial y}+\frac{\partial \psi_y}{\partial x}\right), \tag{20b}$$

$$M_{xy} = B_{16}\left(\frac{\partial u}{\partial x}+\frac{1}{2}\left(\frac{\partial w}{\partial x}\right)^2\right)+B_{26}\left(\frac{\partial v}{\partial y}+\frac{1}{2}\left(\frac{\partial w}{\partial y}\right)^2\right)+B_{66}\left(\frac{\partial u}{\partial y}+\frac{\partial v}{\partial x}+\frac{\partial w}{\partial x}\frac{\partial w}{\partial y}\right)$$
$$+D_{16}\frac{\partial \psi_x}{\partial x}+D_{26}\frac{\partial \psi_y}{\partial y}+D_{66}\left(\frac{\partial \psi_x}{\partial y}+\frac{\partial \psi_y}{\partial x}\right), \tag{20c}$$

$$Q_{xx} = A_{55}\left(\frac{\partial w}{\partial x}+\psi_x\right)+A_{45}\left(\frac{\partial w}{\partial y}+\psi_y\right), \tag{21a}$$

$$Q_{yy} = A_{45}\left(\frac{\partial w}{\partial y}+\psi_y\right)+A_{44}\left(\frac{\partial w}{\partial y}+\psi_y\right), \tag{21b}$$

where

$$A_{ij} = \sum_{k=1}^{N}\int_{z^{(k-1)}}^{z^{(k)}} Q_{ij}^{(k)}dz, \qquad (i,j=1,2,6) \tag{22}$$

$$B_{ij} = \sum_{k=1}^{N}\int_{z^{(k-1)}}^{z^{(k)}} Q_{ij}^{(k)}z dz, \tag{23}$$

$$D_{ij} = \sum_{k=1}^{N}\int_{z^{(k-1)}}^{z^{(k)}} Q_{ij}^{(k)}z^2 dz, \tag{24}$$

Substituting Eqs. (19)-(21) into Eqs. (14)-(18) yields the governing equations as

$$A_{11}\left(\frac{\partial^2 u}{\partial x^2}+\frac{\partial w}{\partial x}\frac{\partial^2 w}{\partial x^2}\right)+A_{12}\left(\frac{\partial^2 v}{\partial x\,\partial y}+\frac{\partial w}{\partial y}\frac{\partial^2 w}{\partial x\,\partial y}\right)+A_{16}\left(\frac{\partial^2 u}{\partial x\,\partial y}+\frac{\partial^2 v}{\partial x^2}+\frac{\partial w}{\partial y}\frac{\partial^2 w}{\partial x^2}+\frac{\partial w}{\partial x}\frac{\partial^2 w}{\partial x\,\partial y}\right)$$
$$+B_{11}\frac{\partial^2 \psi_x}{\partial x^2}+B_{12}\frac{\partial^2 \psi_y}{\partial x\,\partial y}+B_{16}\left(\frac{\partial^2 \psi_x}{\partial x\,\partial y}+\frac{\partial^2 \psi_y}{\partial x^2}\right)+A_{16}\left(\frac{\partial^2 u}{\partial x\,\partial y}+\frac{\partial w}{\partial x}\frac{\partial^2 w}{\partial x\,\partial y}\right)+A_{26}\left(\frac{\partial^2 v}{\partial y^2}+\frac{\partial w}{\partial y}\frac{\partial^2 w}{\partial y^2}\right) \tag{25}$$

$$+A_{66}\left(\frac{\partial^2 u}{\partial y^2}+\frac{\partial^2 v}{\partial x\,\partial y}+\frac{\partial w}{\partial x}\frac{\partial^2 w}{\partial y^2}+\frac{\partial w}{\partial y}\frac{\partial^2 w}{\partial x\,\partial y}\right)+B_{16}\frac{\partial^2 \psi_x}{\partial x\,\partial y}+B_{26}\frac{\partial^2 \psi_y}{\partial y^2}+B_{66}\left(\frac{\partial^2 \psi_x}{\partial y^2}+\frac{\partial^2 \psi_y}{\partial x\,\partial y}\right)=0, \quad (25)$$

$$\begin{aligned}&A_{16}\left(\frac{\partial^2 u}{\partial x^2}+\frac{\partial w}{\partial x}\frac{\partial^2 w}{\partial x^2}\right)+A_{26}\left(\frac{\partial^2 v}{\partial x\,\partial y}+\frac{\partial w}{\partial y}\frac{\partial^2 w}{\partial x\,\partial y}\right)+A_{66}\left(\frac{\partial^2 u}{\partial x\,\partial y}+\frac{\partial^2 v}{\partial x^2}+\frac{\partial w}{\partial y}\frac{\partial^2 w}{\partial x^2}+\frac{\partial w}{\partial x}\frac{\partial^2 w}{\partial x\,\partial y}\right)\\&+B_{16}\frac{\partial^2 \psi_x}{\partial x^2}+B_{26}\frac{\partial^2 \psi_y}{\partial x\,\partial y}+B_{66}\left(\frac{\partial^2 \psi_x}{\partial x\,\partial y}+\frac{\partial^2 \psi_y}{\partial x^2}\right)+A_{21}\left(\frac{\partial^2 u}{\partial x\,\partial y}+\frac{\partial w}{\partial x}\frac{\partial^2 w}{\partial x\,\partial y}\right)+A_{22}\left(\frac{\partial^2 v}{\partial y^2}+\frac{\partial w}{\partial y}\frac{\partial^2 w}{\partial y^2}\right)\\&+A_{26}\left(\frac{\partial^2 u}{\partial y^2}+\frac{\partial^2 v}{\partial x\,\partial y}+\frac{\partial w}{\partial x}\frac{\partial^2 w}{\partial y^2}+\frac{\partial w}{\partial y}\frac{\partial^2 w}{\partial x\,\partial y}\right)+B_{21}\frac{\partial^2 \psi_x}{\partial x\,\partial y}+B_{22}\frac{\partial^2 \psi_y}{\partial y^2}+B_{26}\left(\frac{\partial^2 \psi_x}{\partial y^2}+\frac{\partial^2 \psi_y}{\partial x\,\partial y}\right)=0,\end{aligned} \quad (26)$$

$$\begin{aligned}&A_{55}\left(\frac{\partial^2 w}{\partial x^2}+\frac{\partial \psi_x}{\partial x}\right)+A_{45}\left(\frac{\partial^2 w}{\partial x\,\partial y}+\frac{\partial \psi_y}{\partial x}\right)+A_{45}\left(\frac{\partial^2 w}{\partial x\,\partial y}+\frac{\partial \psi_x}{\partial y}\right)+A_{44}\left(\frac{\partial^2 w}{\partial y^2}+\frac{\partial \psi_y}{\partial y}\right)\\&+N_{xx}^{M}\frac{\partial^2 w}{\partial x^2}+N_{yy}^{M}\frac{\partial^2 w}{\partial x^2}-k_w w+k_g\left(\frac{\partial^2 w}{\partial x^2}+\frac{\partial^2 w}{\partial y^2}\right)=0,\end{aligned} \quad (27)$$

$$\begin{aligned}&B_{11}\left(\frac{\partial^2 u}{\partial x^2}+\frac{\partial w}{\partial x}\frac{\partial^2 w}{\partial x^2}\right)+B_{12}\left(\frac{\partial^2 v}{\partial x\,\partial y}+\frac{\partial w}{\partial y}\frac{\partial^2 w}{\partial x\,\partial y}\right)+B_{16}\left(\frac{\partial^2 u}{\partial x\,\partial y}+\frac{\partial^2 v}{\partial x^2}+\frac{\partial w}{\partial y}\frac{\partial^2 w}{\partial x^2}+\frac{\partial w}{\partial x}\frac{\partial^2 w}{\partial x\,\partial y}\right)\\&+D_{11}\frac{\partial^2 \psi_x}{\partial x^2}+D_{12}\frac{\partial^2 \psi_y}{\partial x\,\partial y}+D_{16}\left(\frac{\partial^2 \psi_x}{\partial x\,\partial y}+\frac{\partial^2 \psi_y}{\partial x^2}\right)+B_{16}\left(\frac{\partial^2 u}{\partial x\,\partial y}+\frac{\partial w}{\partial x}\frac{\partial^2 w}{\partial x\,\partial y}\right)+B_{26}\left(\frac{\partial^2 v}{\partial y^2}+\frac{\partial w}{\partial y}\frac{\partial^2 w}{\partial y^2}\right)\\&+B_{66}\left(\frac{\partial^2 u}{\partial y^2}+\frac{\partial^2 v}{\partial x\,\partial y}+\frac{\partial w}{\partial x}\frac{\partial^2 w}{\partial y^2}+\frac{\partial w}{\partial y}\frac{\partial^2 w}{\partial x\,\partial y}\right)+D_{16}\frac{\partial^2 \psi_x}{\partial x\,\partial y}+D_{26}\frac{\partial^2 \psi_y}{\partial y^2}+D_{66}\left(\frac{\partial^2 \psi_x}{\partial y^2}+\frac{\partial^2 \psi_y}{\partial x\,\partial y}\right)\\&-A_{55}\left(\frac{\partial w}{\partial x}+\psi_x\right)-A_{45}\left(\frac{\partial w}{\partial y}+\psi_y\right)=0,\end{aligned} \quad (28)$$

$$\begin{aligned}&B_{16}\left(\frac{\partial^2 u}{\partial x^2}+\frac{\partial w}{\partial x}\frac{\partial^2 w}{\partial x^2}\right)+B_{26}\left(\frac{\partial^2 v}{\partial x\,\partial y}+\frac{\partial w}{\partial y}\frac{\partial^2 w}{\partial x\,\partial y}\right)+B_{66}\left(\frac{\partial^2 u}{\partial x\,\partial y}+\frac{\partial^2 v}{\partial x^2}+\frac{\partial w}{\partial y}\frac{\partial^2 w}{\partial x^2}+\frac{\partial w}{\partial x}\frac{\partial^2 w}{\partial x\,\partial y}\right)\\&+D_{16}\frac{\partial^2 \psi_x}{\partial x^2}+D_{26}\frac{\partial^2 \psi_y}{\partial x\,\partial y}+D_{66}\left(\frac{\partial^2 \psi_x}{\partial x\,\partial y}+\frac{\partial^2 \psi_y}{\partial x^2}\right)+B_{21}\left(\frac{\partial^2 u}{\partial x\,\partial y}+\frac{\partial w}{\partial x}\frac{\partial^2 w}{\partial x\,\partial y}\right)+B_{22}\left(\frac{\partial^2 v}{\partial y^2}+\frac{\partial w}{\partial y}\frac{\partial^2 w}{\partial y^2}\right)\\&+B_{26}\left(\frac{\partial^2 u}{\partial y^2}+\frac{\partial^2 v}{\partial x\,\partial y}+\frac{\partial w}{\partial x}\frac{\partial^2 w}{\partial y^2}+\frac{\partial w}{\partial y}\frac{\partial^2 w}{\partial x\,\partial y}\right)+D_{21}\frac{\partial^2 \psi_x}{\partial x\,\partial y}+D_{22}\frac{\partial^2 \psi_y}{\partial y^2}+D_{26}\left(\frac{\partial^2 \psi_x}{\partial y^2}+\frac{\partial^2 \psi_y}{\partial x\,\partial y}\right)\\&-A_{45}\left(\frac{\partial w}{\partial y}+\psi_y\right)-A_{44}\left(\frac{\partial w}{\partial y}+\psi_y\right)=0,\end{aligned} \quad (29)$$

5. DQM

In this method, the differential equations are changed into a first order algebraic equation by employing appropriate weighting coefficients. In other words, the partial derivatives of a function

(say f here) are approximated with respect to specific variables (say x and y), at a discontinuous point in a defined domain ($0 < x < a$ and $0 < y < b$) as a set of linear weighting coefficients and the amount represented by the function itself at that point and other points throughout the domain. The approximation of the nth and mth derivatives function with respect to x and y, respectively may be expressed as (Kolahchi *et al*. 2016a, b)

$$\begin{aligned} f_x^{(n)}(x_i, y_i) &= \sum_{k=1}^{N_x} A^{(n)}{}_{ik} f(x_k, y_j), \\ f_y^{(m)}(x_i, y_i) &= \sum_{l=1}^{N_y} B^{(m)}{}_{jl} f(x_i, y_l), \\ f_{xy}^{(n+m)}(x_i, y_i) &= \sum_{k=1}^{N_x} \sum_{l=1}^{N_y} A^{(n)}{}_{ik} B^{(m)}{}_{jl} f(x_k, y_l), \end{aligned} \tag{30}$$

where N_x and N_y, denotes the number of points in x and y directions, $f(x, y)$ is the function and A_{ik}, B_{jl} are the weighting coefficients defined as

$$\begin{aligned} A^{(1)}{}_{ij} &= \frac{M(x_i)}{(x_i - x_j) M(x_j)}, \\ B^{(1)}{}_{ij} &= \frac{P(y_i)}{(y_i - y_j) M(y_j)}, \end{aligned} \tag{31}$$

where M and P are Lagrangian operators defined as

$$\begin{aligned} M(x_i) &= \prod_{j=1}^{N_x} (x_i - x_j), \quad i \neq j \\ P(y_i) &= \prod_{j=1}^{N_y} (y_i - y_j), \quad i \neq j. \end{aligned} \tag{32}$$

The weighting coefficients for the second, third and fourth derivatives are determined via matrix multiplication

$$\begin{aligned} A^{(2)}{}_{ij} &= \sum_{k=1}^{N_x} A^{(1)}{}_{ik} A^{(1)}{}_{kj}, \; A^{(3)}{}_{ij} = \sum_{k=1}^{N_x} A^{(2)}{}_{ik} A^{(1)}{}_{kj}, \; A^{(4)}{}_{ij} = \sum_{k=1}^{N_x} A^{(3)}{}_{ik} A^{(1)}{}_{kj}, \quad i, j = 1,2,..., N_x, \\ B^{(2)}{}_{ij} &= \sum_{k=1}^{N_y} B^{(1)}{}_{ik} B^{(1)}{}_{kj}, \; B^{(3)}{}_{ij} = \sum_{k=1}^{N_y} B^{(2)}{}_{ik} B^{(1)}{}_{kj}, \; B^{(4)}{}_{ij} = \sum_{k=1}^{N_y} B^{(3)}{}_{ik} B^{(1)}{}_{kj}, \quad i, j = 1,2,..., N_y. \end{aligned} \tag{33}$$

Using the following rule, the distribution of grid points in domain is calculated as

$$x_i = \frac{a}{2}\left[1 - \cos\left(\frac{\pi i}{N_x}\right)\right], \qquad y_j = \frac{b}{2}\left[1 - \cos\left(\frac{\pi j}{N_y}\right)\right], \tag{34}$$

Using Eq. (30), and assuming $N_{xx}^{M} = -P$ and $N_{yy}^{M} = -kP$, the governing equations can be expressed in matrix form as

$$\left(\left[K_L + K_{NL} \right] + P \left[K_g \right] \right) \{ d \} = 0 \tag{35}$$

where $[K_G]$ is the coefficient force matrix, $[K_L]$ is the linear stiffness matrix and $[K_{NL}]$ is the nonlinear stiffness matrix and $\{d\} = \{u, v, w, \psi_x, \psi_y\}$ is the displacement vector. This nonlinear equation can now be solved using a direct iterative process as follows:

- First, nonlinearity is ignored by taking $K_{NL} = 0$ to solve the eigenvalue problem expressed in Eq. (35). This yields the linear eigenvalue (P_L) and associated eigenvector (d). The eigenvector is then scaled up so that the maximum transverse displacement of the structure is equal to the maximum eigenvector, i.e., the given vibration amplitude $d_{\max}$.
- Using linear d, $[K_{NL}]$ can be evaluated. Eigenvalue problem is then solved by substituting $[K_{NL}]$ into Eq. (35). This would give the nonlinear eigenvalue (P_{NL}) and the new eigenvector.
- The new nonlinear eigenvector is scaled up again and the above procedure is repeated iteratively until the buckling load values from the two subsequent iterations ‘ r ‘ and ‘ $r+1$ ‘ satisfy the prescribed convergence criteria as $\dfrac{\left| \omega^{r+1} - \omega^{r} \right|}{\omega^{r}} < \varepsilon_0$

where ε_0 is a small value number and in the present analysis it is taken to be 0.01%.

6. Numerical results

In this section, a laminated plate with the material properties listed in Table 1 is considered.

At the first, the convergence and accuracy of proposed method are studied. Then, the results are validated with other published works and finally, the effects of different parameters such as number of lamina, orientation angle of lamina, volume percent of SWCNTs, SWCNTs agglomeration, boundary conditions, elastic medium and axial mode number of plate are shown on the dimensionless buckling load ($DBL = P/(E_{11}a)$). Three kinds of boundary conditions: all edges simply supported (SSSS) or clamped (CCCC), and two opposite edges simply supported and the other two clamped (SCSC) (Kolahchi *et al*. 2016a)

Table 1 Material properties of Graphite/Epoxy (Phung-Van *et al*. 2015c)

Properties	Value
E_{11}	132.38 GPa
$E_{22} = E_{33}$	10.76 GPa
G_{12}	3.61 GPa
$G_{13} = G_{23}$	5.65 GPa
$v_{11} = v_{23}$	0.24
v_{13}	0.49

6.1 DQM convergence

Fig. 2 shows the accuracy and convergence of DQM. In this figure, the dimensionless buckling load is plotted versus axial mode numbers for different grid points number in x and y directions. It can be seen that with increasing the number of grid points, the dimensionless buckling load is decreased until in $N_x = N_y = 15$, the results are converged. However, in the present work, the numbers of grid points are selected to be 15.

6.2 Validation

In order to validate the present results, we neglected from the agglomerated SWCNTs as reinforcement ($C_r = \xi = \zeta = 0$), elastic medium constants ($k_w = k_g = 0$) and nonlinear term in governing equations. However, the buckling of simply supported a laminated plate is studied based on FSDT and DQM. Considering the material properties the same as Matsunaga (2000). The results of comparison are shown in Table 2. As can be seen, the present results are in good agreement with Noor (1975) based on 3D elasticity solution, Putcha and Reddy (1986) based on FSDT and Matsunaga (2000) based on HSDT. Noted that the little difference between the results of this work and other works is due to the difference in the theory and solution method.

6.3 The effect of different parameters

In all of the following figures, the dimensionless buckling load is plotted against axial mode number. It can be observed that the buckling load decreases at first until reaches to the lowest amount and after that increasing process begins. The critical buckling load appears in the point where the buckling load is minimal. Noted that this phenomenon is reported by other researchers (Kadoli and Ganesan 2003, Han 2009, Sheng and Wang 2010, Chan *et al*. 2011, Zhu and Li 2016), indicating validation of presented figures.

The effect of the SWCNTs volume percent on the dimensionless buckling load versus the axial

Table 2 Comparison of present work with the published papers

No. of layers	Solution	E_1/E_2				
		3	10	20	30	40
3	A	5.3044	9.7621	15.0191	19.3040	22.8807
	B	5.3991	9.9652	15.3510	19.7560	23.4530
	C	5.3208	9.7172	14.7290	18.6834	21.8977
	D	5.3918	9.8452	14.9167	18.8769	22.1531
5	A	5.3255	9.9603	15.6527	20.4663	24.5929
	B	5.4093	10.1360	15.9560	20.9080	25.1850
	C	5.3348	9.9414	15.5142	20.1656	24.1158
	D	3.4011	9.9087	15.2451	20.3483	24.9098

A: 3D elasticity solution, Noor (1975)
B: FSDT, Putcha and Reddy (1986)
C: HSDT, Matsunaga (2000)
D: Present work

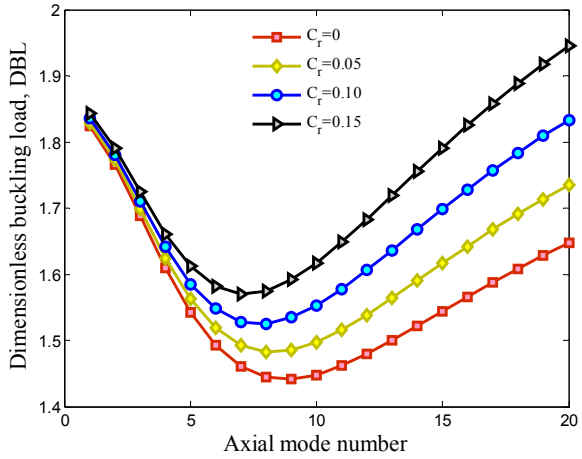

Fig. 2 The effect of SWCNTs volume percent on the dimensionless buckling load versus axial mode number

mode number is shown in Fig. 3. It can be found that with increasing the SWCNTs volume percent, the dimensionless buckling load increases and the critical buckling load is increased. It is due to the fact that with increasing SWCNTs volume percent, the stiffness of the structure increases. In addition, the effect of SWCNTs volume percent on the dimensionless buckling load becomes more prominent at higher axial mode numbers.

In order to show the effects of SWCNTs agglomeration on the dimensionless buckling load, Fig. 4 is plotted. As can be seen, considering agglomeration effects leads to decrease in the dimensionless buckling load of the structure. It is because that the SWCNTs agglomeration is an harmful parameters for system due to reduction in the stability and rigidity of the structure. However, since the dispersion of SWCNTs in the matrix cannot be uniform in real, the results of this figure can be useful for the researchers and design of laminated plates with nanocomposite layers.

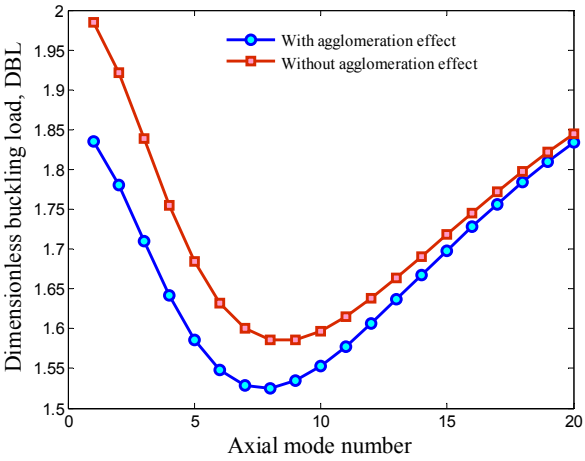

Fig. 3 The effect of SWCNTs agglomeration on the dimensionless buckling load versus axial mode number

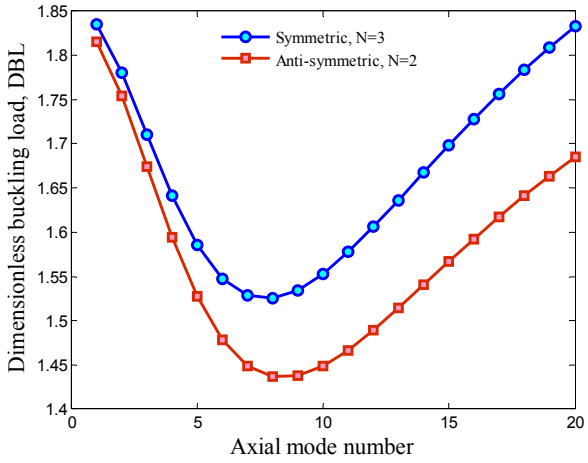

Fig. 4 The effect of lamina numbers on the dimensionless buckling load versus axial mode number

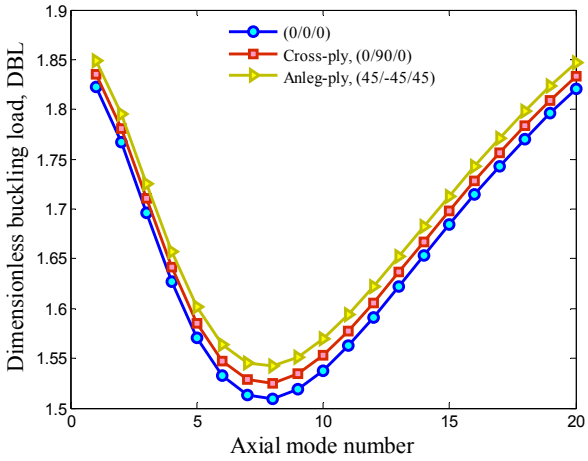

Fig. 5 The effect of orientation angle of layers on the dimensionless buckling load versus axial mode number

Fig. 5 illustrates the effect of the layers number on the dimensionless buckling load versus axial mode numbers. It can be concluded that the symmetric structure with 3 layers number predicted the higher dimensionless buckling load for all axial mode numbers with respect to the anti-symmetric one with 2 layers number. It is due to the fact that stability and balance of structure with symmetric laminas are higher than those of anti-symmetric one.

The effect of the orientation angle of the SWCNTs in the laminas is presented in Fig 6 on the dimensionless buckling load versus axial mode number. Here, three cases of (0°, 0°, 0°), cross-ply lamina (0°, 90°, 0°) and angle-ply lamina (45°, –45°, 45°) are assumed. As can be seen, the dimensionless buckling load for the angle-ply lamina is higher than cross-ply and zero laminas. In other words, the zero lamina predicts the lowest dimensionless buckling load with respect to other cases.

Fig. 7 demonstrates the effect of boundary conditions on the dimensionless buckling load versus axial mode number. Three boundary conditions of SSSS, SCSC and CCCC are considered.

It is obvious that the dimensionless buckling load has the following order for the proposed boundary conditions: CCCC > SCSC > SSSS

Hence, the laminated plate with CCCC has the higher dimensionless buckling load with respect to other considered cases. It is due to the fact that the stiffness of structure increases for the CCCC boundary condition.

The effect of the elastic medium is shown in Fig. 8 on the dimensionless buckling load versus axial mode number. Generally the existence of the elastic medium increases the stiffness of the structure and thereby the dimensionless buckling load increases. The Pasternak medium considers the vertical and shear loads however the Winkler medium considers only the vertical ones, therefore the effect of Pasternak medium is more than Winkler medium. According to Fig. 5, the effect of the elastic medium on the buckling load is significant and it can be a useful parameter to take away the system from buckling condition.

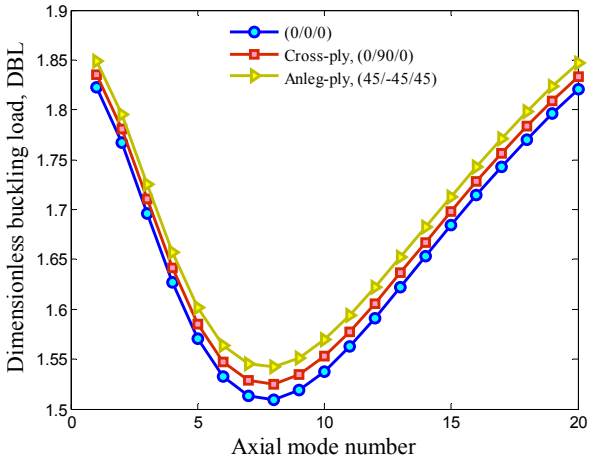

Fig. 6 The effect of boundary conditions on the dimensionless buckling load versus axial mode number

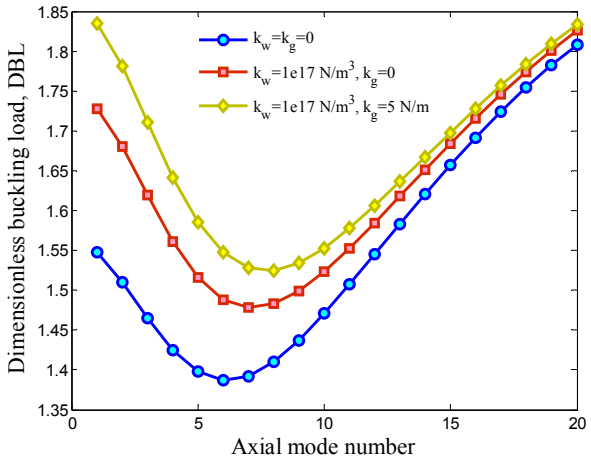

Fig. 7 The effect of elastic medium on the dimensionless buckling load versus axial mode number

7. Conclusions

Buckling analysis of embedded laminated plates with nanocomposite layers was investigated in this article. The lamina layers were reinforced with SWCNTs considering agglomeration effects. Based on the FSDT, the governing equations were derived using energy method and Hamilton's principal. In order to obtain the buckling load, DQM was performed for three boundary conditions. The effects of elastic medium, volume percent of SWCNTs, SWCNTs agglomeration, boundary conditions, number of layers and orientation angle of layers on the buckling of the structure were considered. Results indicate that considering SWCNTs agglomeration decreases the buckling load of the structure. Increasing the volume percent of SWCNTs increases the buckling load of the laminated plate. In addition, the CCCC boundary condition leads to higher buckling load with respect to the SCSC and SSSS boundary conditions. Furthermore, the angle-ply lamina with the symmetric layer numbers increases the bucking load of system. Present results were in a good agreement with other published works. Finally, it is hoped that the results presented in this paper would be helpful for study and design of rectangular laminated plates with nanocomposite layers.

References

Chan, Y., Thamwattana, N. and Hill, J.M. (2011), "Axial buckling of multi-walled carbon nanotubes and nanopeapods", *Eur. J. Mech. A/Solids*, **30**(6), 794-806.

El-Hassar, S.M., Benyoucef, S., Heireche, H. and Tounsi, A. (2016), "Thermal stability analysis of solar functionally graded plates on elastic foundation using an efficient hyperbolic shear deformation theory", *Geomech. Eng., Int. J.*, **10**(3), 357-386.

Han, H.C. (2009), "Blood vessel buckling within soft surrounding tissue generates tortuosity", *J. Biomech.*, **42**(16), 2797-2801.

Heydari, M.M., Kolahchi, R., Heydari, M. and Abbasi, A. (2014), "Exact solution for transverse bending analysis of embedded laminated Mindlin plate", *Struct. Eng. Mech., Int. J.*, **49**(5), 661-672.

Kadoli, R. and Ganesan, N. (2003), "Free vibration and buckling analysis of composite cylindrical shells conveying hot fluid", *Compos. Struct.*, **60**(1), 19-32.

Kolahchi, R., Safari, M. and Esmailpour, M. (2016a), "Dynamic stability analysis of temperature-dependent functionally graded CNT-reinforced visco-plates resting on orthotropic elastomeric medium", *Compos. Struct.*, **150**, 255-265.

Kolahchi, R., Hosseini, H. and Esmailpour, M. (2016b), "Differential cubature and quadrature-Bolotin methods for dynamic stability of embedded piezoelectric nanoplates based on visco-nonlocal-piezoelasticity theories", *Compos. Struct.*, **157**, 174-186.

Luong-Van, H., Nguyen-Thoi, T., Liu, G.R. and Phung-Van, P. (2014), "A cell-based smoothed finite element method using three-node shear-locking free Mindlin plate element (CS-FEM-MIN3) for dynamic response of laminated composite plates on viscoelastic foundation", *Eng. Anal. Bound. Elem.*, **42**, 8-19.

Matsunaga, H. (2000), "Vibration and stability of cross-ply laminated composite plates according to a global higher-order plate theory", *Compos. Struct.*, **48**(4), 231-244.

Nguyen-Thoi, T., Luong-Van, H., Phung-Van, P., Rabczuk, T. and Tran-Trung, D. (2013), "Dynamic responses of composite plates on the Pasternak Foundation subjected to a moving mass by a cell-based smoothed discrete shear gap (CS-FEM-DSG3) method", *Int. J. Compos. Mat.*, **3**, 19-27.

Nguyen-Thoi, T., Rabczuk, T., Lam-Phat, T., Ho-Huu, V. and Phung-Van, P. (2014a), "Free vibration analysis of cracked Mindlin plate using an extended cell-based smoothed discrete shear gap method (XCS-DSG3)", *Theoret. Appl. Fract. Mech.*, **72**, 150-163.

Nguyen-Thoi, T., Bui-Xuan, T., Phung-Van, P., Nguyen-Hoang, S. and Nguyen-Xuan, H. (2014b), "An edge-based smoothed three-node mindlin plate element (ES-MIN3) for static and free vibration analyses

of plates", *KSCE J. Civil Eng*., **18**(4), 1072-1082.
Nguyen, X.H., Nguyen, N.T., Abdel Wahab, M., Bordas, S.P.A., Nguyen-Xuan, H. and Voa, P.T. (2017), "A refined quasi-3D isogeometric analysis for functionally graded microplates based on the modified couple stress theory", *Comput. Meth. Appl. Mech. Eng*., **313**, 904-940.
Noor, A.K. (1975), "Stability of multilayered composite plates", *Fibre Sci. Tech*., **8**(2), 81-89.
Phung-Van, P., Luong-Van, H., Nguyen-Thoi, T. and Nguyen-Xuan, H. (2014a), "A cell-based smoothed discrete shear gap method (CS-FEM-DSG3) based on the C0-type higher-order shear deformation theory for dynamic responses of Mindlin plates on viscoelastic foundations subjected to a moving sprung vehicle", *Int. J. Numeric. Meth. Eng*., **98**(13), 988-1014.
Phung-Van, P., Nguyen-Thoi, T., Luong-Van, H., Thai-Hoang, C. and Nguyen-Xuan, H. (2014b), "A cell-based smoothed discrete shear gap method (CS-FEM-DSG3) using layerwise deformation theory for dynamic response of composite plates resting on viscoelastic foundation", *Comput. Meth. Appl. Mech. Eng*., **272**, 138-159.
Phung-Van, P., Thai, C.H., Nguyen-Thoi, T. and Nguyen-Xuan, H. (2014c), "Static and free vibration analyses of composite and sandwich plates by an edge-based smoothed discrete shear gap method (ES-DSG3) using triangular elements based on layerwise theory", *Compos. Part B*: *Eng*., **60**, 227-238.
Phung Van, P., Abdel Wahab, M., Liew, K.M., Bordas, S.P.A. and Nguyen-Xuan, H. (2015a), "Isogeometric analysis of functionally graded carbon nanotube-reinforced composite plates using higher-order shear deformation theory", *Compos. Struct*., **123**, 137-149.
Phung Van, P., Nguyen, L.B., Tran, V.L., Dinh, T.D., Thai, C.H., Bordas, S.P.A., Abdel-Wahab, M. and Nguyen-Xuan, H. (2015b), "An efficient computational approach for control of nonlinear transient responses of smart piezoelectric composite plates", *Int. J. Non-Linear Mech*., **76**, 190-202.
Phung-Van, P., De Lorenzis, L., Thai, Ch.H., Abdel-Wahab, M. and Nguyen-Xuan, H. (2015c), "Analysis of laminated composite plates integrated with piezoelectric sensors and actuators using higher-order shear deformation theory and isogeometric finite elements", *Comput. Mat. Sci*., **96**, 495-505.
Phung-Van, P., Tran, L.V., Ferreira, A.J.M., Nguyen-Xuan, H. and Abdel-Wahab, M. (2016), "Nonlinear transient isogeometric analysis of smart piezoelectric functionally graded material plates based on generalized shear deformation theory under thermo-electro-mechanical loads", *Nonlinear Dyn*., **87**(2), 879-894. DOI: 0.1007/s11071-016-3085-6
Putcha, N.S. and Reddy, J.N. (1986), "Stability and natural vibration analysis of laminated plates by using a mixed element based on a refined plate theory", *J. Sound Vib*., **104**(2), 285-300.
Reddy, J.N. (1984), "A simple higher order theory for laminated composite plates", *J. Appl. Mech*., **51**(4), 745-752.
Saidi, H., Tounsi, A. and Bousahla, A.A. (2016), "A simple hyperbolic shear deformation theory for vibration analysis of thick functionally graded rectangular plates resting on elastic foundations", *Geomech. Eng*., *Int. J*., **11**(2), 289-307.
Sheng, G.G. and Wang, X. (2010), "Response and control of functionally graded laminated piezoelectric shells under thermal shock and moving loadings", *Compos. Struct*., **93**(6), 132-141.
Shi, D**.**L**.**and Feng, X**.**Q**.** (2004), "The effect of nanotube waviness and agglomeration on the lastic property of carbon nanotube-reinforced composties", *J. Eng. Mat. Tech. ASME*, **126**(3), 250-270.
Thai, C.H., Ferreira, A.J.M., Abdel Wahab, M. and Nguyen-Xuan, H. (2016a), "A generalized layerwise higher-order shear deformation theory for laminated composite and sandwich plates based on isogeometric analysis", *Acta Mech*., **227**(5), 1225-1250.
Thai, C., Zenkour, A.M., Abdel Wahab, M. and Nguyen-Xuan, H. (2016b), "A simple four-unknown shear and normal deformations theory for functionally graded isotropic and sandwich plates based on isogeometric analysis", *Compos. Struct*., **139**, 77-95.
Tran, V.L., Lee, J., Ly, H.A., Abdel Wahab, M. and Nguyen-Xuan, H. (2015a), "Vibration analysis of cracked FGM plates using higher-order shear deformation theory and extended isogeometric approach", *Int. J. Mech. Sci*., **96**, 65-78.
Tran, V.L., Lee, J., Nguyen-Van, H., Nguyen-Xuan, H. and Abdel Wahab, M. (2015b), "Geometrically nonlinear isogeometric analysis of laminated composite plates based on higher-order shear deformation

theory", *Int. J. Non-Linear Mech.*, **72**, 42-52.
Tran, L.V., Phung-Van, P., Lee, J., Abdel Wahab, A. and Nguyen-Xuan, H. (2016), "Isogeometric analysis for nonlinear thermomechanical stability of functionally graded plates", *Compos. Struct.*, **140**, 655-667.
Zhu, J. and Li, L.Y. (2016), "A stiffened plate buckling model for calculating critical stress of distortional buckling of CFS beams", *Int. J. Mech. Sci.*, **115-116**, 457-464.

CC

Appendix A

Hence, the effective bulk modulus (K) and effective shear modulus (G) may be written as

$$K = K_{out}\left[1+\frac{\xi\left(\frac{K_{in}}{K_{out}}-1\right)}{1+\alpha\left(1-\xi\right)\left(\frac{K_{in}}{K_{out}}-1\right)}\right], \tag{A1}$$

$$G = G_{out}\left[1+\frac{\xi\left(\frac{G_{in}}{G_{out}}-1\right)}{1+\beta\left(1-\xi\right)\left(\frac{G_{in}}{G_{out}}-1\right)}\right], \tag{A2}$$

where

$$K_{in} = K_m + \frac{\left(\delta_r - 3K_m\chi_r\right)C_r\zeta}{3\left(\xi - C_r\zeta + C_r\zeta\chi_r\right)}, \tag{A3}$$

$$K_{out} = K_m + \frac{C_r\left(\delta_r - 3K_m\chi_r\right)\left(1-\zeta\right)}{3\left[1-\xi-C_r\left(1-\zeta\right)+C_r\chi_r\left(1-\zeta\right)\right]}, \tag{A4}$$

$$G_{in} = G_m + \frac{\left(\eta_r - 3G_m\beta_r\right)C_r\zeta}{2\left(\xi - C_r\zeta + C_r\zeta\beta_r\right)}, \tag{A5}$$

$$G_{out} = G_m + \frac{C_r\left(\eta_r - 3G_m\beta_r\right)\left(1-\zeta\right)}{2\left[1-\xi-C_r\left(1-\zeta\right)+C_r\beta_r\left(1-\zeta\right)\right]}, \tag{A6}$$

where χ_r, β_r, δ_r, η_r may be calculated as

$$\chi_r = \frac{3\left(K_m+G_m\right)+k_r-l_r}{3\left(k_r+G_m\right)}, \tag{A7}$$

$$\beta_r = \frac{1}{5}\left\{\frac{4G_m+2k_r+l_r}{3\left(k_r+G_m\right)}+\frac{4G_m}{\left(p_r+G_m\right)}+\frac{2\left[G_m\left(3K_m+G_m\right)+G_m\left(3K_m+7G_m\right)\right]}{G_m\left(3K_m+G_m\right)+m_r\left(3K_m+7G_m\right)}\right\}, \tag{A8}$$

$$\delta_r = \frac{1}{3}\left[n_r+2l_r+\frac{\left(2k_r-l_r\right)\left(3K_m+2G_m-l_r\right)}{k_r+G_m}\right], \tag{A9}$$

$$\eta_r = \frac{1}{5}\left[\frac{2}{3}\left(n_r - l_r\right) + \frac{4G_m p_r}{\left(p_r + G_m\right)} + \frac{8G_m m_r\left(3K_m + 4G_m\right)}{3K_m\left(m_r + G_m\right) + G_m\left(7m_r + G_m\right)} + \frac{2\left(k_r - l_r\right)\left(2G_m + l_r\right)}{3\left(k_r + G_m\right)}\right]. \tag{A10}$$

where k_r, l_r, n_r, p_r, m_r are the Hills elastic modulus for the nanoparticles; K_m and G_m are the bulk and shear moduli of the matrix which can be written as

$$K_m = \frac{E_m}{3\left(1-2\upsilon_m\right)}, \tag{A11}$$

$$G_m = \frac{E_m}{2\left(1+\upsilon_m\right)}. \tag{A12}$$

Furthermore, β, α can be obtained from

$$\alpha = \frac{\left(1+\upsilon_{out}\right)}{3\left(1-\upsilon_{out}\right)}, \tag{A13}$$

$$\beta = \frac{2\left(4-5\upsilon_{out}\right)}{15\left(1-\upsilon_{out}\right)}, \tag{A14}$$

$$\upsilon_{out} = \frac{3K_{out} - 2G_{out}}{6K_{out} + 2G_{out}}. \tag{A15}$$

Appendix B

Q_{ij} (i, j = 1, 2,..., 6) are defined as

$$Q_{11} = C_{11}\cos^4\theta - 4C_{16}\cos^3\theta\sin\theta + 2(C_{12} + 2C_{66})\cos^2\theta\sin^2\theta - 4C_{26}\cos\theta\sin^3\theta + C_{22}\sin^4\theta, \tag{B1}$$

$$Q_{12} = C_{12}\cos^4\theta + 2(C_{16} - C_{26})\cos^3\theta\sin\theta + (C_{11} + C_{22} - 4C_{66})\cos^2\theta\sin^2\theta + 2(C_{26} - C_{16})\cos\theta\sin^3\theta + C_{12}\sin^4\theta, \tag{B2}$$

$$Q_{16} = C_{16}\cos^4\theta + (C_{11} - C_{12} - 2C_{66})\cos^3\theta\sin\theta + 3(C_{26} - C_{16})\cos^2\theta\sin^2\theta + (2C_{66} + C_{12} - C_{22})\cos\theta\sin^3\theta - C_{26}\sin^4\theta, \tag{B3}$$

$$Q_{22} = C_{22}\cos^4\theta + 4C_{26}\cos^3\theta\sin\theta + 2(C_{12} + 2C_{66})\cos^2\theta\sin^2\theta + 4C_{16}\cos\theta\sin^3\theta + C_{11}\sin^4\theta, \tag{B4}$$

$$Q_{26} = C_{26}\cos^4\theta + (C_{12} - C_{22} + 2C_{66})\cos^3\theta\sin\theta + 3(C_{16} - C_{26})\cos^2\theta\sin^2\theta + (C_{11} - C_{12} - 2C_{66})\cos\theta\sin^3\theta - C_{16}\sin^4\theta, \tag{B5}$$

$$Q_{66} = 2(C_{16} - C_{26})\cos^3\theta\sin\theta + (C_{11} + C_{22} - 2C_{12} - 2C_{66})\cos^2\theta\sin^2\theta + 2(C_{26} - C_{26})\cos\theta\sin^3\theta + C_{66}(\cos^4\theta + \sin^4\theta), \tag{B6}$$

$$Q_{44} = C_{44}\cos^2\theta + 2C_{45}\cos\theta\sin\theta + C_{55}\sin^2\theta, \tag{B7}$$

$$Q_{45} = (C_{55} - C_{44})\cos\theta\sin\theta + C_{44}(\cos^2\theta - \sin^2\theta), \tag{B8}$$

$$Q_{55} = C_{55}\cos^2\theta - 2C_{45}\cos\theta\sin\theta + C_{44}\sin^2\theta, \tag{B9}$$

where C_{ij} (i, j = 1, 2,..., 6) denotes elastic coefficients and θ is orientation angle.